THE ASTROPHYSICAL JOURNAL, 503:938–952, 1998 August 20
© 1998. The American Astronomical Society. All rights reserved. Printed in U.S.A.

QUANTITATIVE MAGNETOHYDRODYNAMIC MODELING OF THE SOLAR TRANSITION REGION

MICHAEL L. GOODMAN
Computer Sciences Corporation and Laboratory for Extraterrestrial Physics, Code 695, NASA Goddard Space Flight Center, Greenbelt, MD 20771;
goodman@spof02.gsfc.nasa.gov
Received 1997 September 10; accepted 1998 March 30

ABSTRACT

The transition region (TR) is assumed to be a collision-dominated plasma. The dissipation and transport of energy in such a plasma is accurately described by the classical transport coefficients, which include the electrical and thermal conductivity, viscosity, and thermoelectric tensors. These tensors are anisotropic and are functions of local values of temperature, density, and magnetic field strength. The transport coefficients are valid for all magnetic field strengths and so may be used to study the physics of weakly as well as strongly magnetized regions of the TR. They may be used in an MHD model to obtain a self-consistent, realistic description of the TR. The physics of kinetic processes is included in the MHD model through the transport coefficients. As a first step in studying heating and cooling processes in the TR in a realistic, quantitative manner, a 1.5 dimensional, steady state MHD model with a specified temperature profile is developed. The momentum equation includes the inertial, pressure, magnetic, and gravitational forces. Ohm's law includes the exact expressions for the electrical conductivity and thermoelectric tensors. It is found that the contribution of the dissipation of large-scale electric currents to in situ heating of the TR is negligible, but that thermal energy flowing into the TR from the corona can provide the energy required to heat the TR. The possibility that significant in situ heating of the TR takes place through viscous dissipation or small-scale electric current dissipation such as may occur in current sheets or filaments is discussed, although these processes are not described by the model. The importance of thermoelectric and electron pressure gradient effects in Ohm's law, and in determining the electron heat flux, is demonstrated. Results of the model suggest that the force-free approximation is not valid over most of the TR. Justification for assuming that the TR is collision dominated is presented. In particular, a self-consistent calculation of the ratio of the electric field parallel to the magnetic field to the Dreicer electric field yields a value $\lesssim 10^{-3}$, which suggests that anomalous transport processes are not important. The necessity of using a realistic description of transport processes in modeling heating mechanisms in the solar atmosphere is stressed.

Subject headings: MHD — Sun: magnetic fields — Sun: transition region

1. INTRODUCTION

The identification and understanding of the mechanisms responsible for heating the chromosphere, transition region (TR), and corona of the Sun and other solar type stars is a major problem in solar and stellar physics. The work presented here addresses part of this problem, namely heating of the solar TR. This work is complementary to ongoing work on chromospheric heating by Goodman (1995, 1996, 1997a, 1997b) and is part of a long-term program to develop MHD models using realistic transport coefficients to study energy dissipation and transport in the solar atmosphere. Any proposed heating mechanism is important in some region of parameter space, but the critical question is whether it is valid in the region of parameter space that describes the solar atmosphere. This question can be answered only by an analysis based on a realistic model of the proposed heating mechanism that makes *numerical predictions* of heating rates, energy fluxes, and profiles of important quantities such as density, temperature, velocity, and electric and magnetic fields. Only by developing such models and comparing their predictions with what is observed in the solar atmosphere can its heating mechanisms be identified and understood. This paper presents what appears to be the first model of this type for the TR.

The solar TR (Mariska 1986, 1992) is that part of the solar atmosphere lying between the chromosphere, which has a temperature $T < 2 \times 10^4$ K and where hydrogen is weakly or moderately ionized, and the corona, which has a temperature $T \sim 10^6$ K and where hydrogen is fully ionized. The structure of the TR is largely determined by the magnetic field. The TR may be divided into the lower transition region (LTR), defined by the temperature range 2×10^4 K $\leq T \leq 2.5 \times 10^5$ K, and the upper transition region (UTR), defined by the temperature range 2.5×10^5 K $\leq T \leq 10^6$ K. One-dimensional, semiempirical, hydrostatic, non-LTE models of the TR that do not include effects due to flow or electric and magnetic fields (see, e.g., Fontenla, Avrett, & Loeser 1991, 1993; Mariska 1992) indicate that its height range is less than that of the chromosphere and that it is an almost isobaric region in which the proton density decreases from $\sim 10^{11}$ to 10^9 cm^{-3} as the temperature increases from $\sim 10^4$ to 10^6 K with increasing height. This class of models predicts that the TR height range is $\lesssim 10^2$ km. However, observations of rapid downflows of material at TR temperatures suggest that its height range is $\gg 10^2$ km (Foukal 1990), and there are limb observations that indicate that the TR emission between 4×10^4 K and 2.2×10^5 K is distributed over a height range of several thousand kilometers (§ 3.2 of Mariska 1992). The height range of the TR may vary widely over the surface of the Sun and may be very different from the values predicted by hydrostatic models. Consistent with the current prevailing view of the TR, its height range for the model used here, determined by the temperature profile and constraints specified in § 2.2.6, is found to be ~ 86 km, with the understanding that this value may have to be significantly revised

as observational resolution and modeling accuracy improve.

During "explosive events," flow speeds in the TR can surge to ~ 100 km s^{-1} (Dere, Bartoe, & Brueckner 1984). By contrast, the quiet TR exhibits Doppler redshifts up to ~ 17 km s^{-1}, and smaller blueshifts, with the size of the redshift positively correlated with the strength of the underlying photospheric magnetic field, especially in the supergranulation network (Brynildsen, Kjeldseth-Moe, & Maltby 1996; Mariska 1988). However, nonthermal speeds possibly associated with wave motion, rather than bulk flow, up to ~ 30 km s^{-1} are observed (Warren et al. 1997).

Like the chromosphere and corona, the TR is heated by unknown sources of energy that power its net radiative loss (NRL). Observations indicate that the TR consists of a mixture of hot and cool magnetic loops (Athay & Dere 1991; Dowdy 1993; Dowdy, Rabin, & Moore 1986), with large temperature gradients on scales as small as 1″ (~ 720 km) or less driving a thermal energy flux between hot and cool loops. The NRL from the TR is almost entirely UV/EUV emission, and the more intense emission appears to come from the neutral line region of heated magnetic bipoles. Recent *SOHO* observations support this picture (S. D. Jordan 1997, private communication). These observations are consistent with early sounding-rocket observations of the X-ray corona over active regions, which indicate that the emission intensities peak over the magnetic neutral lines of the underlying photospheric magnetic field (Vaiana, Krieger, & Timothy 1973).

The plasma in the TR is composed of ionized hydrogen together with a relatively small fraction of ions and neutral hydrogen. The mass and momentum flux in the TR is carried almost entirely by protons, and electric currents are carried almost entirely by electrons. Although the ions and neutral hydrogen make a negligible contribution to mass and momentum transport, and to the current density, they are responsible for almost all of the NRL.

The NRL in the EUV is observed to fluctuate on all resolvable spatial scales by 10%–30% on a timescale of minutes in quiet network and in cell centers (Rabin & Dowdy 1992). According to Rabin & Dowdy (1992), these fluctuations are not associated with fluctuations in the thermal energy flux down from the corona, and are likely caused by small-scale fluctuations in the magnetic field. This suggests that the TR is at least partially heated by an in situ mechanism that involves the magnetic field. The small to moderate size of the intensity fluctuations suggests that they represent a small to moderate perturbation of a primary driver of the heating mechanism that is quasi-steady on timescales of several minutes.

The NRL is powered by some combination of in situ thermal energy generation and externally generated thermal energy flowing into it. The NRL is $\sim 4 \times 10^5$ ergs cm^{-2} s^{-1}, with almost 75% of this flux coming from the LTR (Dowdy et al. 1986). At present there are three main, partially conflicting views of the thermal energy source of the NRL. The first view is that the source is thermal conduction of energy down from the corona (Fontenla et al. 1991, 1993). In this view, there is little or no in situ heating in the TR. The second view is that the LTR is heated in situ, and that the UTR is heated by thermal conduction of energy down from the corona (Dowdy 1993; Dowdy et al. 1986; Rabin & Moore 1984). Rabin & Moore (1984) suggest that the LTR is heated in situ by the classical resistive dissipation of magnetic field–aligned electric currents flowing in cylindrical current channels with diameters of ~ 1 km. The third view (Scudder 1994) is that the TR and corona are heated by the thermalization of particles in the high-energy tails of non-Maxwellian distribution functions formed by an unknown mechanism in the upper chromosphere at a temperature of $\sim 1.4 \times 10^4$ K. The importance of non-Maxwellian distribution functions in the TR is a controversial issue (Anderson, Raymond, & van Ballegooijen 1996; Anderson 1994; Scudder 1994; Macneice, Fontenla, & Ljepojevic 1991). For the model presented here, it is assumed that the velocity distribution functions in the TR are close to Maxwellian, in which case transport processes are accurately described by the classical transport coefficients, which are well-known functions of number density, temperature, and magnetic field strength. A subset of these transport coefficients, together with a specified temperature profile, is used in a 1.5 dimensional MHD model to obtain numerical estimates of heating rates due to current dissipation and the influx of thermal energy from the corona, and to compute profiles of pressure, density, velocity, electric and magnetic fields, and current density as a function of height in an 86 km thick TR. By definition, in a 1.5 dimensional model, all quantities vary only with a single spatial variable, in this case the height variable, and the three components of vector quantities are allowed to be nonzero. The justification for using classical transport coefficients is presented in § 2.1.

2. DESCRIPTION OF THE MODEL

2.1. *Justification of the Use of Classical Transport Coefficients*

There are various estimates of the conditions under which the classical transport coefficients are valid (see, e.g., Balescu 1988a; Book 1990; Mitchner & Kruger 1973). Four of these conditions are not obviously satisfied in the TR and so must be checked.

The first condition is that the timescales of interest be much longer than the proton-proton collision time. For the TR the largest value of this collision time is ~ 2 s. Since only equilibrium states are considered here this condition need not be discussed further.

The second condition is that the thermal mean free path $l_{\rm mfp}$ be much less than the smallest of the values of the characteristic lengths over which the temperature, density, velocity, and magnetic and electric fields undergo significant variation parallel to the magnetic field and the length $L_{\rm B}$ of magnetic field lines in the TR. More accurately, if $l_{\parallel}$ measures distance along a field line, one must have $l_{\rm mfp} \ll$ minimum $[L_{\rm B}, Q/(dQ/dl_{\parallel})]$ at any point in the TR, where Q represents temperature, density, and any component of the velocity, electric, or magnetic field, and $L_{\rm B}$ refers to the length in the TR of the field line passing through that point. For the model solutions presented in § 4, the mean free path increases monotonically from ~ 40 cm to ~ 93 km over the derived 86 km height range of the TR. For these solutions, the magnetic field is nearly horizontal, and by assumption all quantities can vary only in the vertical direction. It follows that the condition $l_{\rm mfp} \ll Q/(dQ/dl_{\parallel})$ is satisfied. It remains to check that $l_{\rm mfp} \ll L_{\rm B}$. The horizontal length scales that characterize variations in MHD variables are expected to be much larger than the height range of the TR under the assumption, consistent with observation, that the temperature and density vary much more rapidly in the

vertical than in the horizontal direction. Then the characteristic *minimum* length of field lines in the TR is on the order of the TR height range. For a nearly constant TR pressure of ~ 0.55 dyn cm^{-2}, which characterizes the solutions presented in § 4, and a Coulomb logarithm of 10, $l_{\rm mfp} \sim 9.32 \times 10^{-17} T(K)^3$ km. The mean free path decreases rapidly with decreasing temperature. For the solutions presented in § 4, $l_{\rm mfp}$ equals one-half the height range of the TR at a height ~ 44 km and a temperature of $\sim 7.8 \times 10^5$ K. These estimates suggest that $l_{\rm mfp}$ is significantly less than the characteristic length of magnetic field lines throughout most of the TR. In particular, this inequality certainly holds in the LTR, where $T \leq 2.5 \times 10^5$ K, $l_{\rm mfp} \lesssim 1.5$ km and where $\sim 75\%$ of TR heating occurs (Dowdy et al. 1986). Then the second condition is satisfied in the LTR and is at least marginally satisfied in the UTR.

Let $R_{i,L}$ be the ion Larmor radius. Then the third condition is that $(R_{i,L} l_{\rm mfp})^{1/2}$ be much less than the smallest of the values of the TR height range H, and the characteristic lengths over which the temperature, density, velocity, and magnetic and electric fields undergo significant variation in any direction orthogonal to the magnetic field. More accurately, if $l_\perp$ measures distance from a field line in a direction orthogonal to the field, one must have $(R_{i,L} l_{\rm mfp})^{1/2} \ll$ minimum $[H, Q/(dQ/dl_\perp)]$ at any point in the TR, where Q represents temperature, density, and any component of the velocity, electric, or magnetic field. For the solutions presented in § 4, the magnetic field strength and pressure are nearly constant. In this case $(R_{i,L} l_{\rm mfp})^{1/2} \propto T^{7/4}$, and its maximum value of ~ 0.22 km occurs at the top of the TR where $T = 10^6$ K. By comparison, for the solutions presented in § 4, the largest value of $Q/(dQ/dl_\perp)$ occurs for $Q = T$ at the base of the TR, where $T = 2 \times 10^4$ K, and $T/(dT/dl_\perp)$ ~ 0.88 km. Then the third condition is satisfied.

The fourth condition is that anomalous (i.e., wave-particle or collisionless) transport processes not be important. Anomalous transport processes are not well understood, but a reasonable measure of their importance is the ratio of $E_\parallel$, the magnitude of the electric field parallel to $\boldsymbol{B}$, to the Dreicer electric field $E_{\rm D}$ (Dreicer 1959; Balescu 1988b; de Kluiver, Perepelkin, & Hirose 1991). Essentially, $E_{\rm D}$ is the electric field necessary to accelerate an electron from zero speed to the thermal speed in one collision time, or equivalently in one mean free path. The electron-proton collision frequency decreases with increasing electron speed so that when $E_\parallel/E_{\rm D}$ exceeds a critical value, electron runaway causes an initially near Maxwellian electron velocity distribution function to develop a high-energy tail large enough to invalidate the use of classical transport coefficients. A detailed analysis by Balescu (1988b, § 19.2) indicates that this critical value is ~ 0.21. As long as $E_\parallel/E_{\rm D} \ll$ 0.21, it is unlikely that anomalous transport processes are important. Only solutions to the model that satisfy this inequality are acceptable. For the solutions presented in § 4, the range of this ratio is $10^{-6} \lesssim E_\parallel/E_{\rm D} \lesssim 10^{-3}$. Then the fourth condition is satisfied. In particular, in the LTR of these solutions, $E_\parallel/E_{\rm D} \leq 3.5 \times 10^{-4}$.

$E_{\rm D}$ is a function only of density and temperature. The density and temperature ranges of the TR are fairly well known from observation (Mariska 1992) and are close to those in the model presented here. For the range of $E_{\rm D}$ corresponding to the model solutions in § 4, it follows that near the base of the TR one needs $E_\parallel \sim 3.7$ V m^{-1} and near the top of the TR one needs $E_\parallel \sim 2.5 \times 10^{-3}$ V m^{-1} in order that $E_\parallel/E_{\rm D} \sim 0.21$ in these regions. By comparison, for the solutions in § 4, the magnitude of $E_\parallel$ is $\sim 5.3 \times 10^{-5}$ V m^{-1} near the base of the TR, and $\sim 6.9 \times 10^{-9}$ V m^{-1} near the top of the TR. Any acceptable in situ TR heating mechanism that is based on anomalous dissipation mechanisms must include a realistic mechanism for generating parallel electric fields that are strong enough to violate the condition $E_\parallel/E_{\rm D} \ll 0.21$. The existence of such fields in the TR, especially on the meter to kilometer scales believed to characterize current sheets and filaments, cannot at present be ruled out, although a convincing mechanism for generating them has not yet been proposed.

Semiempirical evidence that the TR is collision dominated is provided by Fontenla et al. (1991, 1993) and Macneice et al. (1991). Fontenla et al. (1991, 1993) model the LTR up to $T = 10^5$ K using a one-dimensional, semiempirical, hydrostatic, non-LTE model. They assume that the LTR is collision dominated and that the downward energy flux from the corona accounts for all of the NRL of the LTR. Under these assumptions, they obtain order of magnitude agreement between computed and measured H and He I and He II spectra. Macneice et al. (1991) test the basic assumptions of Fontenla et al. (1991) and extend their model up to $T = 10^6$ K using a Fokker-Planck model. They show that, for 10^5 K $\leq T \leq 10^6$ K, the effects of a high-energy non-Maxwellian tail on the heat flux and the ionization state of elements in the TR is negligible, and the downward conductive heat flux computed from their Fokker-Planck model is very close to the heat flux predicted using the classical expression for the electron thermal conductivity.

Although the most recent model of Fontenla et al. (1993) does not include effects due to flow or electric and magnetic fields, it does include important effects due to radiative transfer, and the ambipolar diffusion of ions and electrons with respect to neutral atoms in the TR. The model presented here includes the former effects but not the latter. In this sense the two models are complementary. Both models assume that the LTR is collision dominated, and therefore that the local particle distribution functions are close to Maxwellian. The first-order departures of the distribution functions from a Maxwellian one give rise to the classical transport processes.

In the corona over active regions, where the most intense heating occurs, observations by Landini & Landini (1997) and Brosius et al. (1996) imply densities of $\sim 10^9$–10^{10} cm^{-3} and corresponding temperatures of ~ 1–5×10^6 K, with the higher temperatures generally corresponding to the higher densities. The corresponding range of the mean free path is ~ 100–500 km. Over quiet regions of the corona, observations by Brosius et al. (1996) imply $T \sim 1$–2×10^6 K and $n \sim 10^9$ cm^{-3}, which are close to the values at the top of the TR for the model solutions presented in § 4. These observations are consistent with the view that the UTR and low corona is the region where anomalous transport processes begin to dominate over classical transport processes, but where classical transport processes may still be important.

The discussion in this section indicates that the LTR, which is the region of the most intense radiative loss, is strongly collision dominated, and it suggests that classical transport processes play an important, if not dominant, role in the UTR. As one moves from the TR into the corona, although the temperature increases slowly to values that are typically no more than a few million degrees, the density

can rapidly decrease by several orders of magnitude. In that case, since the mean free path is $\propto T^2/n$, where n is the density, it rapidly increases to 10^3–10^4 km, approaching the dimensions of the thickness and height range of heated coronal loops. For such long mean free paths, the collision-dominated approximation is almost certainly not valid, and collisionless transport processes are expected to be dominant.

2.2. *Basic Equations*

The complete set of MHD equations, together with the expressions for the classical transport coefficients valid for all magnetic field strengths, is derived in detail from first principles by Balescu (1988a) for a plasma of electrons and positive ions of arbitrary charge. The derivation of Balescu is an extension and correction of the original derivation given by Braginskii (1965). A simplified version of these equations is used here. The transport coefficients are tensors that describe transport of energy, momentum, and charge parallel and perpendicular to the magnetic field. They are functions of temperature, density, and magnetic field strength that are functions of height in the model presented here. Hence the transport coefficients vary with height in the TR and are computed self-consistently in the model. Their values can vary by many orders of magnitude over the height range of the TR, as shown in § 4.2.5. The transport coefficients are anisotropic, and their components that describe transport parallel and perpendicular to the magnetic field can differ by orders of magnitude. Therefore a self-consistent calculation of all elements of the transport coefficients provides a far more accurate description of the physics of the TR than is obtained by assuming that the transport coefficients are constant or isotropic. Taking into account the inhomogeneity and anisotropy of the transport coefficients is critically important when trying to determine whether a proposed heating mechanism can provide the required heating rate for the TR when the heating rate is computed using realistic ranges for temperature, density, electric and magnetic field strength, and flow speed that characterize the TR.

In this first attempt to model the TR using realistic transport coefficients in an MHD model, a 1.5 dimensional, steady state model is used together with the following additional simplifying assumptions. The TR plasma is assumed to be a fully ionized electron-proton plasma. In Cartesian coordinates x, y, z, all quantities vary with height z above the base of the TR, taken to be at $z = 0$. The temperature profile is specified, so there is no energy equation. The effects of viscosity are omitted in the momentum equation. Unless indicated otherwise, cgs units are used.

The basic equations are the commonly used MHD equations with the exception of Ohm's law (eq. [11]), and the expression for the electron heat flux (eq. [17]). These equations contain thermoelectric and electron pressure effects that are usually neglected. Solutions to the model show that these effects are important and so should not be neglected.

For the model under consideration, in which all quantities can depend only on z, the MHD equations are as follows.

2.2.1. *Maxwell's Equations*

$$B_z = B_z(0) \tag{1}$$

$$E_x = E_x(0) \tag{2}$$

$$E_y = E_y(0) \tag{3}$$

$$J_x = -\frac{c}{4\pi} B_y' \tag{4}$$

$$J_y = \frac{c}{4\pi} B_x' \tag{5}$$

$$J_z = 0\,, \tag{6}$$

where $\boldsymbol{E}$, $\boldsymbol{B}$, $\boldsymbol{J}$, and c are the electric and magnetic fields, current density, and speed of light. $B_z(0)$, $E_x(0)$, and $E_y(0)$ are to be specified. Equation (1) follows from $\nabla \cdot \boldsymbol{B} = 0$, equations (2) and (3) follow from $\nabla \times \boldsymbol{E} = 0$, and equations (4), (5), and (6) follow from $\boldsymbol{J} = c\nabla \times \boldsymbol{B}/(4\pi)$. Equation (6), which states that the vertical current density is zero, is used in the z component of Ohm's law, equation (11), to obtain an equation for $E_z(z)$.

2.2.2. *Mass Conservation*

The mass conservation equation reduces to the statement that the vertical mass flux is constant.

$$\rho V_z = M_0\,, \tag{7}$$

where M_0, ρ, and V_z are the vertical mass flux, mass density, and z component of the bulk velocity $\boldsymbol{V}$. M_0 is an input to the model and may be positive or negative to model upward- or downward-flowing plasma.

2.2.3. *Momentum Conservation*

Neglecting the effects of viscosity, the momentum equation reduces to

$$M_0 V_x - \frac{B_x B_z}{4\pi} = M_0 V_x(0) - \frac{B_x(0) B_z}{4\pi} \tag{8}$$

$$M_0 V_y - \frac{B_y B_z}{4\pi} = M_0 V_y(0) - \frac{B_y(0) B_z}{4\pi} \tag{9}$$

$$M_0 V_z' + p' = -\frac{1}{4\pi}\left(B_x B_x' + B_y B_y'\right) - \rho g_\odot\,, \tag{10}$$

where p and $g_\odot$ are the pressure and gravitational acceleration at 1 $R_\odot$. The prime indicates differentiation with respect to z.

2.2.4. *Ohm's Law*

$$\boldsymbol{J} = \boldsymbol{\sigma} \cdot \boldsymbol{E}_{\rm eff} - \boldsymbol{\alpha} \cdot \nabla T \tag{11}$$

$$\equiv \boldsymbol{J}_{\rm conduction} + \boldsymbol{J}_{\rm thermoelectric} \tag{12}$$

where T, $\boldsymbol{\sigma}$, $\boldsymbol{\alpha}$, e, n, and $\boldsymbol{E}_{\rm eff}$ are the temperature, electrical conductivity and thermoelectric tensors (see Appendix A), magnitude of the electron charge, number density, and effective electric field defined by

$$\boldsymbol{E}_{\rm eff} \equiv \boldsymbol{E} + \frac{\boldsymbol{V} \times \boldsymbol{B}}{c} + \frac{\nabla p}{2en}\,. \tag{13}$$

In equation (11) the effective electric field drives the conduction current density, and the temperature gradient drives the thermoelectric current density.

In the numerical examples presented in § 4, the horizontal (x and y) components of $\boldsymbol{J}_{\rm conduction}$ and $\boldsymbol{J}_{\rm thermoelectric}$ have opposite signs and, as discussed in § 4.2.3, largely cancel one another over most of the TR, indicating that thermoelectric effects are important in determining the current density in

the TR. Although equation (6) states that the vertical current density must be zero, and hence that the vertical components of the thermoelectric and conduction current densities must cancel exactly, there is no constraint that the horizontal components of the thermoelectric and conduction current densities must cancel. The high degree of cancellation of the horizontal components of the thermoelectric and conduction current densities suggests that the TR plasma tends to relax to a state with nearly zero current density, at least on the large scale of the TR height range.

Ohm's law (eq. [11]) is in fact the electron momentum equation with the inertial, viscous, and gravity terms neglected. The pressure gradient term in equation (11) is related to the gradient of the electron pressure p_e by the equation $p_e = p/2$. The x and y components of Ohm's law provide differential equations for B_y and B_x while the z component of Ohm's law, which, using equation (6), enforces the constraint that the vertical component of the current density is zero, provides an algebraic equation for E_z.

2.2.5. *Equation of State*

The electrons and protons are assumed to obey ideal gas equations of state, and the quasi-neutrality condition is assumed to hold. Then

$$p = \frac{2\rho k_B T}{m_p} , \tag{14}$$

where k_B and m_p are Boltzmann's constant and the proton mass.

2.2.6. *Assumed Temperature Profile*

A temperature profile quadratic in the height variable z is chosen. z ranges from 0 to H. The temperatures at the base and top of the TR are chosen to be $T(0) = 2 \times 10^4$ K and $T(H) = 10^6$ K, where the height range H of the TR remains to be determined. The temperature gradient with respect to height is observed to be much larger at the base of the TR, where the rapid temperature rise begins, than at the top of the TR, where the temperature is close to or at its maximum value. Consistent with these observations, the following choices are made. $dT/dz = 0$ at $z = H$, and dT/dz at $z = 0$ is chosen to equal the temperature gradient estimated using the table in Fontenla et al. (1993) corresponding to their model F for bright network. Near 2×10^4 K this table gives $dT/dz \sim 2.275 \times 10^4$ K km^{-1}. Given the values of the temperature and its gradient at the base and top of the TR, it follows that $H = 86.15$ km, and the temperature profile is given by

$$T(z) = T(0) + [T(H) - T(0)]\left[2\left(\frac{z}{H}\right) - \left(\frac{z}{H}\right)^2\right] . \tag{15}$$

For given values of $(dT/dz)_{z=0}$ and $T(H) - T(0)$, the height range of the model TR is computed from the equation

$$H = \frac{2[T(H) - T(0)]}{(dT/dz)_{z=0}} . \tag{16}$$

2.2.7. *Electron Heat Flux*

The exact expression for the electron heat flux is

$$\boldsymbol{q}^e = T\boldsymbol{\alpha} \cdot \boldsymbol{E}_{\rm eff} - \boldsymbol{\kappa}^e \cdot \nabla T \tag{17}$$

$$\equiv \boldsymbol{q}^e_{\rm thermoelectric} + \boldsymbol{q}^e_{\rm conductive} , \tag{18}$$

where $\boldsymbol{\kappa}^e$ is the electron thermal conductivity tensor (see Appendix A). According to equation (17), the effective electric field drives the thermoelectric electron heat flux, and the temperature gradient drives the conductive electron heat flux. In the numerical examples presented in § 4, the three components of $\boldsymbol{q}^e_{\rm thermoelectric}$ cancel $\sim 50\%$ of the corresponding components of $\boldsymbol{q}^e_{\rm conductive}$, showing that thermoelectric effects are important in determining the electron heat flux in the TR.

2.2.8. *Proton Heat Flux*

The exact expression for the proton heat flux is

$$\boldsymbol{q}^p = -\boldsymbol{\kappa}^p \cdot \nabla T , \tag{19}$$

where $\boldsymbol{\kappa}^p$ is the proton thermal conductivity tensor (see Appendix A). There is no thermoelectric component to the proton heat flux.

2.2.9. *Semiempirical Estimate of the Net Radiative Loss*

The current dissipation rate predicted by the model solutions is compared with the semiempirical estimate of the NRL presented in Rosner, Tucker, & Vaiana (1978). This estimate is given by

$$\text{NRL (ergs cm}^{-3}\text{ s}^{-1}) = n^2 Q(T) , \tag{20}$$

where

$$\begin{aligned} Q(T) &= 10^{-21.85} (10^{4.3} < T < 10^{4.6}\text{ K}) \\ &= 10^{-31} T^2 (10^{4.6} < T < 10^{4.9}\text{ K}) \\ &= 10^{-21.2} (10^{4.9} < T < 10^{5.4}\text{ K}) \\ &= 10^{-10.4} T^{-2} (10^{5.4} < T < 10^{5.75}\text{ K}) \\ &= 10^{-21.94} (10^{5.75} < T < 10^{6.3}\text{ K}) \\ &= 10^{-17.73} T^{-2/3} (10^{6.3} < T < 10^{7}\text{ K}) . \end{aligned} \tag{21}$$

3. EQUATIONS FOR NUMERICAL SOLUTION

The solution of the basic equations in § 2.2 can be reduced to the solution of three differential equations for the pressure and the x and y components of the magnetic field. These equations are given by

$$B_x' = F_1(p, B_x, B_y; V_x(0), V_y(0), B_z, E_x, E_y, M_0) \tag{22}$$

$$B_y' = F_2(p, B_x, B_y; V_x(0), V_y(0), B_z, E_x, E_y, M_0) \tag{23}$$

$$p' = F_3(p, B_x, B_y; V_x(0), V_y(0), B_z, E_x, E_y, M_0) , \tag{24}$$

where explicit expressions for F_1, F_2, and F_3 are given in Appendix B. The boundary conditions $p(0)$, $B_x(0)$, $B_y(0)$, $V_x(0)$, and $V_y(0)$ must be specified together with the parameters B_z, E_x, E_y, and M_0. Once equations (22), (23), and (24) are solved, all other quantities of interest are determined by algebraic equations.

Nine quantities must be specified to determine the solution, allowing investigation of a wide range of solutions. Only three solutions are discussed in § 4. The main purpose of these solutions is to demonstrate that dissipation of *large-scale* electric currents makes a negligible contribution to TR heating, that the electron heat flux down from the corona may provide all of the energy necessary to heat the TR, and that it is important to take into account thermoelectric and electron pressure gradient effects when modeling the TR. Here the term "large-scale" refers to currents dis-

tributed over a significant fraction of the height range of the TR.

4. NUMERICAL SOLUTIONS

4.1. *General Discussion*

Three solutions are presented in Figures 1–18. The idea behind generating these solutions is to increase the component of the horizontal electric field that is most nearly parallel to $\boldsymbol{B}$ at the base of the TR to see if the heating rate due to current dissipation can be increased to a value comparable to the NRL as estimated using equation (20). $\boldsymbol{B}$ is nearly parallel to the x-axis for these solutions and is imagined to represent the top part of a magnetic loop in a closed field region of the TR. E_x is increased in steps by factors of 10 from one solution to the next. An adaptive-step Runge-Kutta routine is used to solve equations (22), (23), and (24) (Press et al. 1992). The specified, minimum allowed step size is chosen to be less than the minimum value of the electron Larmor radius to ensure that the spatial scales corresponding to the classical transport processes are resolved.

For all solutions, the values of $B_x(0)$, $B_y(0)$, B_z, $n(0)$, M_0, and E_y are chosen to be 30.0 G, 0.1 G, 1.0 G, 10^{11} cm^{-3}, 10^{-10} g cm^{-2} s^{-1}, and 0.482 V m^{-1}. The vertical mass flux M_0 is chosen to be positive, but solutions with downflow are also allowed and remain to be investigated. For solutions 1–3, E_x is chosen to be $-(0.1, 1.0, 10.0)$ V m^{-1}, respectively. It remains to choose $V_x(0)$ and $V_y(0)$ for each solution. It is found that solutions exist only for certain values of these velocity components, and that these values must be specified with an accuracy in the range of 10^{-8} to 10^{-10} km s^{-1} in order to generate solutions that are smooth on the scale of a few kilometers near $z = 0$. In order to generate solutions 1–3, it is initially assumed that $V_x(0) = 5.0$ km s^{-1}. It is found that this value must be slightly altered, and that the corresponding values of $V_y(0)$ must be chosen to satisfy the condition $\boldsymbol{E}_0 \equiv \boldsymbol{E} + \boldsymbol{V} \times \boldsymbol{B}/c = 0$ to a precision of $\sim 10^{-10}$ statvolts cm^{-1}. This condition on $\boldsymbol{E}_0$ is also the reason why $V_x(0)$ and $V_y(0)$ must be specified with such high precision. The exact values of $V_x(0)$ and $V_y(0)$ that are used to generate solutions 1–3 are $[V_x(0), V_y(0)] = (4.995832854, 0.9993727628)$, (4.995860601, 9.993072761), (4.995978312, 99.93007283) km s^{-1}. It is important to note that a large error in the computation of the current density results if $\boldsymbol{E}_0$ is set equal to zero in the model. Although the magnitude of $\boldsymbol{E}_0$ is only $\sim 10^{-10}$ statvolts cm^{-1}, its product with the electrical conductivity tensor in Ohm's law makes a large contribution to the current density.

For the fixed values of $B_x(0)$, $B_y(0)$, B_z, $n(0)$, M_0, and E_y, only the profiles of E_z and V_y differ between the three solutions on the spatial scale of the figures. When E_x is increased, E_z and V_y increase by almost the same factor so that $\boldsymbol{E}_0$ remains $\sim 10^{-10}$ statvolts cm^{-1}. The magnitude of E_x is not increased beyond the value of 10.0 V m^{-1} since larger values cause V_y to exceed 100 km s^{-1}, which is about the upper limit on observed flow speeds in the TR.

4.2. *Discussion of Specific Profiles*

4.2.1. *Temperature, Pressure, and Density*

The assumed temperature profile is shown in Figure 1. The pressure, shown in Figure 2, decreases by only $\sim 1\%$ over the height range of the TR, in agreement with the observation that the TR is an almost isobaric region in which the temperature increases by a factor of ~ 100 while the density, shown in Figure 3, decreases by the same factor.

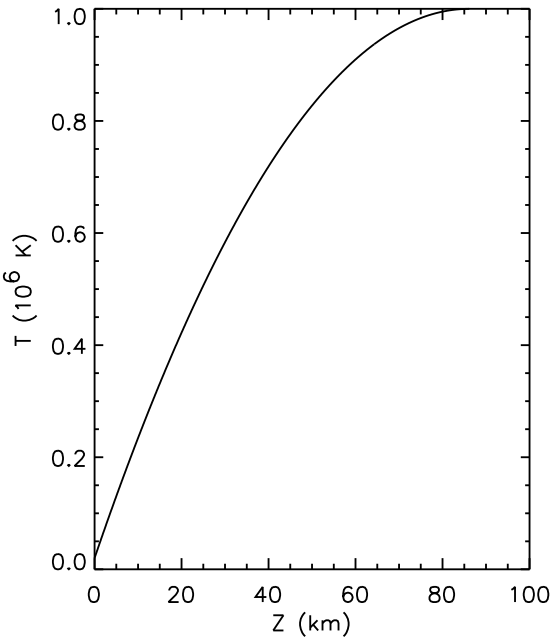


FIG. 1.—Specified temperature profile vs. z

4.2.2. *Magnetic Field and Velocity*

B_x and B_y are shown in Figures 4 and 5. The magnetic field is almost constant, nearly parallel to the x axis, and makes an angle of 88°.1 with the purely vertical temperature gradient. Although B_x and B_y vary on scales of only 10^{-3} and 10^{-6} G, respectively, this relatively small variation corresponds to a horizontal $\boldsymbol{J} \times \boldsymbol{B}$ force, which is balanced by the horizontal inertial forces due to the height variations of V_x and V_y shown in Figures 6 and 7. The balance of these forces is required by the momentum equations (8) and (9). It is necessary to solve for the magnetic field with a high degree of accuracy to accurately calculate the velocity and current density.

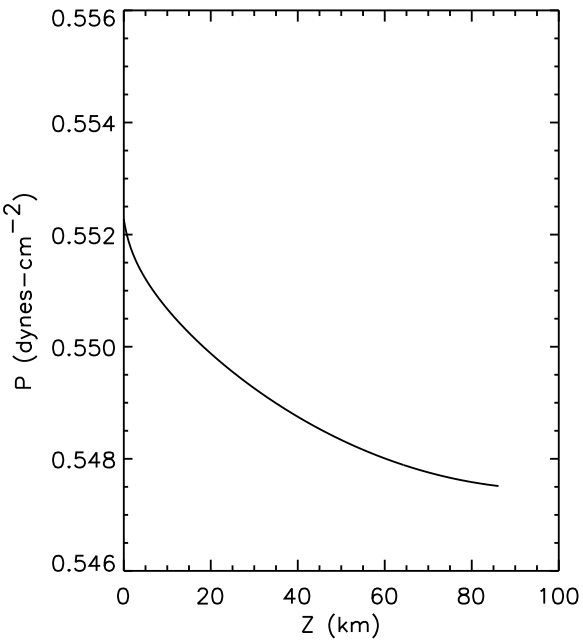


FIG. 2.—Pressure vs. z

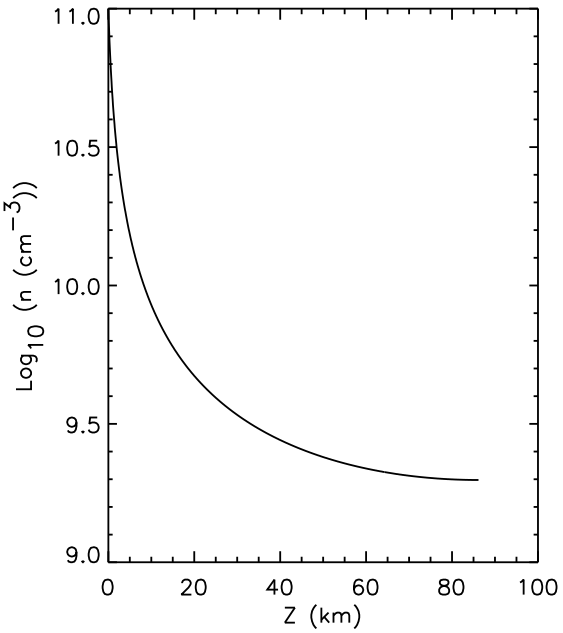


FIG. 3.—Logarithm of the number density vs. z. $n(0)$ is specified

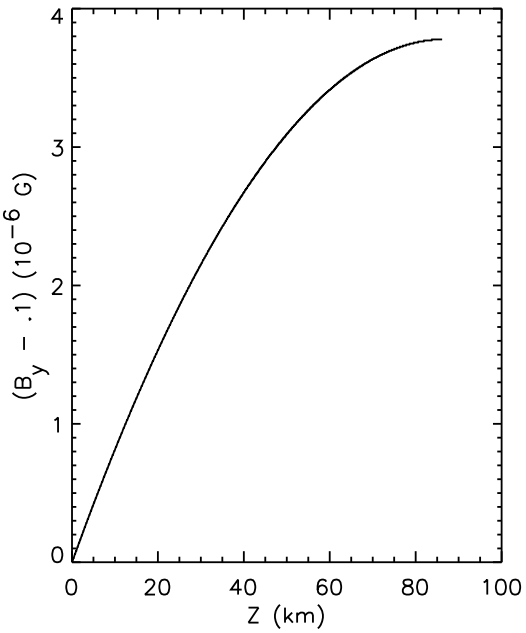


FIG. 5.—y component of magnetic field vs. z. $B_y(0)$ is specified

The vertical component of velocity, shown in Figure 8, increases by a factor of ~ 50 from ~ 6 m s^{-1} at $z = 0$ to ~ 300 m s^{-1} at $z = 86$ km. The mass outflow speed at $z = 86$ km is $\sim 10^3$ times smaller than the solar wind speed at $z \geq 3\ R_\odot$. Unless the TR is much thicker than 86 km, it seems unlikely that substantial solar wind acceleration takes place in the TR in closed field regions. However, the rapid increase of V_z in Figure 8 suggests that much higher outflow speeds at the top of the TR might result from using a much thicker TR. It also remains to be seen if much higher outflow speeds result when the magnetic field is vertical, similar to the open, radial field configuration in coronal holes where the high-speed solar wind is observed.

From solution 1 to solution 3, the flow velocity changes from being mainly parallel to $\boldsymbol{B}$ to being mainly orthogonal to $\boldsymbol{B}$. As E_x is increased by a factor of 10^2 in an attempt to drive a current that generates substantial heating, the flow velocity orthogonal to $\boldsymbol{B}$ increases by the same factor in the y direction. It appears that the flow velocity adjusts itself in response to increases in the electric field to maintain current dissipation at a minimum level.

4.2.3. *Vertical Electric Field and Current Density*

For solutions 1–3, $(E_x, E_y) = (-0.1, 0.482)$, $(-1.0, 0.482)$, $(-10.0, 0.482)$ V m^{-1}. E_z, shown in Figure 9, is essentially constant over the height range of the TR and is $\sim$(3, 30,

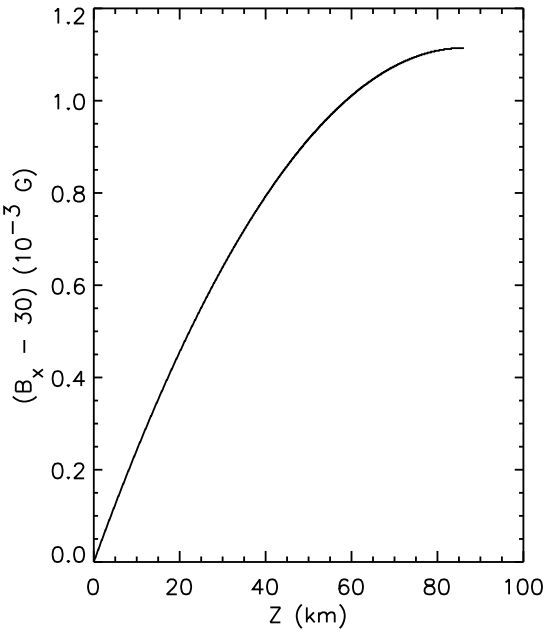


FIG. 4.—x component of magnetic field vs. z. The magnetic field is nearly parallel to the x-axis and is inclined toward the vertical direction by 1°9. $B_x(0)$ and B_z (= 1 G) are specified.

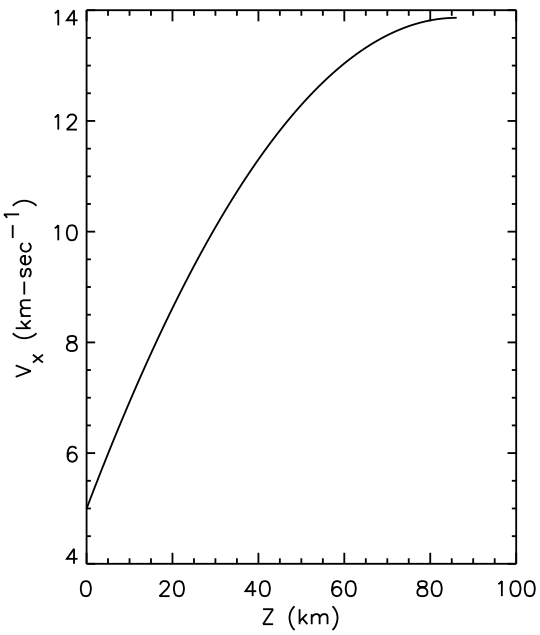


FIG. 6.—x component of velocity vs. z. $V_x(0)$ is specified

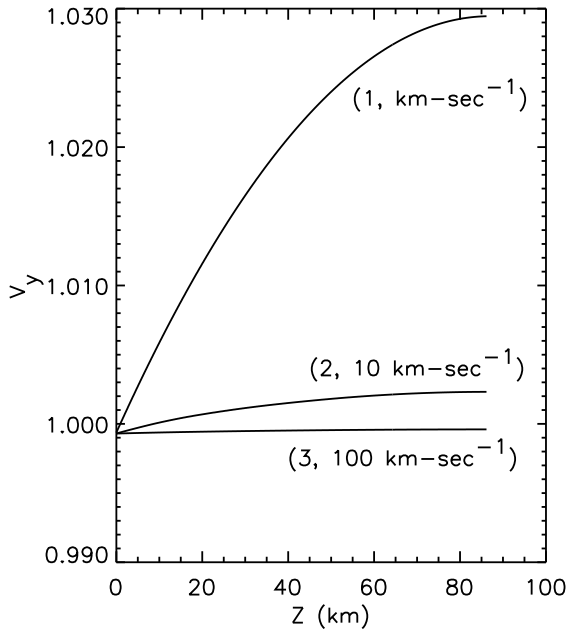


FIG. 7.—y component of velocity vs. z. The solution number and the corresponding units are indicated in parentheses in the figure. $V_y(0)$ is specified.

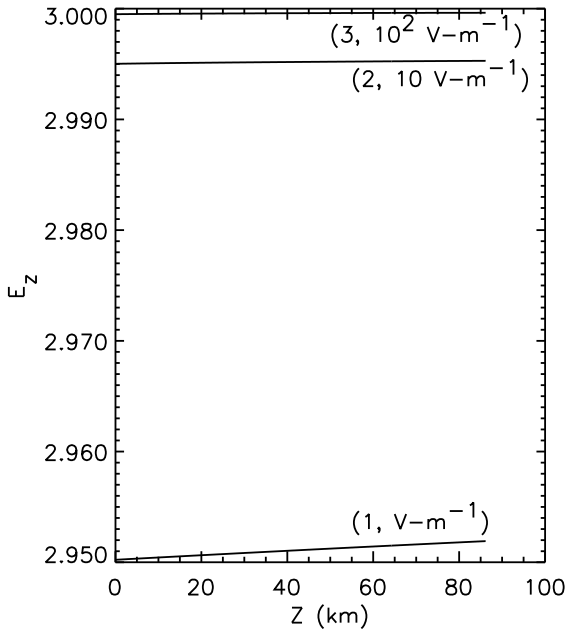


FIG. 9.—z component of electric field vs. z. The solution number, and the corresponding units, are indicated in parentheses in the figure. E_x ($=-0.1$, -1.0, -10.0 V m^{-1} for solutions 1–3) and E_y ($=0.482$ V m^{-1}) are specified.

300) V m^{-1} for solutions 1–3. E_z is the largest component of $\boldsymbol{E}$ by about an order of magnitude. As a result, $\boldsymbol{E}$ is mainly vertical and orthogonal to $\boldsymbol{B}$. Ohm's law (eq. [11]) determines E_z such that the vertical components of the conduction and thermoelectric current density exactly cancel. The relative charge separation is $E'_z/(4\pi en) \lesssim 10^{-15}$, so the assumption of quasi neutrality is justified.

Less is known observationally about the electric field in the solar atmosphere than about any other MHD variable. A major advantage of using a self-consistent model that includes a realistic description of transport processes is that it allows for a realistic calculation of the electric field. The most sensitive observations of electric fields in the solar atmosphere rely on the linear Stark effect in neutral hydrogen and have a resolution of ~ 500 V m^{-1} (Foukal & Hinata 1991). This resolution refers to the magnitude of $\boldsymbol{E} + \boldsymbol{V} \times \boldsymbol{B}/c$, since this is the electric field in the frame of reference of hydrogen atoms moving with the bulk velocity $\boldsymbol{V}$. For the solutions presented here, the magnitude of this field is $\sim 10^{-6}$ V m^{-1}, which is far below the current limit of detection. However, small-scale electric fields, such as are believed to occur in current sheets, may have magnitudes strong enough to cause observable Stark splitting.

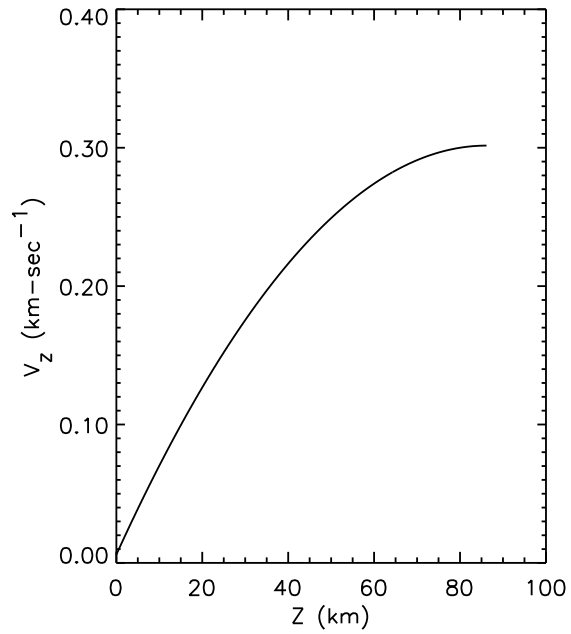


FIG. 8.—z component of velocity vs. z. The vertical mass flux M_0 ($=10^{-10}$ g cm^{-2} s^{-1}) is specified. Together with $n(0)$, this determines $V_z(0)$.

According to Ohm's law (eq. [11]), the current density consists of two parts, a conduction current density driven by the effective electric field (13) and a thermoelectric current density driven by the temperature gradient. For solutions 1–3, the importance of the electron pressure term $p'/(2en)$ in equation (11) is seen by examining the ratio $R \equiv (\boldsymbol{E} + \boldsymbol{V} \times \boldsymbol{B}/c)_z/[p'/(2en)]$. Over the height range of the TR, $-1.0 \leq R < 1.0$ with the magnitude of R largest near the top and bottom of the TR. For $1 \leq z \leq 80$ km, one has $0.65 \geq R \geq -0.5$. The electron pressure term makes the dominant contribution to the z component of the effective electric field throughout the TR.

The current density is almost parallel to $\boldsymbol{B}$, which is almost parallel to the x-axis, and J_x is $\sim$10–100 J_y. J_x and its conduction and thermoelectric components are shown in Figures 10, 11, and 12. The magnitudes of $J_{x,\mathrm{conduction}}$ and $J_{x,\mathrm{thermoelectric}}$ increase rapidly from ~ 192.0 and 191.3 mA m^{-2} at $z = 0$ to values $\sim 10^4$–10^5 times larger than their sum J_x up to $z = 86$ km. From $z = 86$ km to the top of the TR at $z = 86.15$ km, $J_{x,\mathrm{thermoelectric}}$ decreases rapidly to zero since by assumption the temperature gradient is zero at the top of the TR. At $z = 86.15$ km, $J_{x,\mathrm{conduction}} \sim 10^{-2}$ mA m^{-2}. Similarly, $J_{y,\mathrm{conduction}} < 0$, $J_{y,\mathrm{thermoelectric}} > 0$, and their magnitudes increase rapidly from ~ 0.61 and 0.64 mA m^{-2}, respectively, at $z = 0$, to values $\sim 10^4$–10^5 times larger than

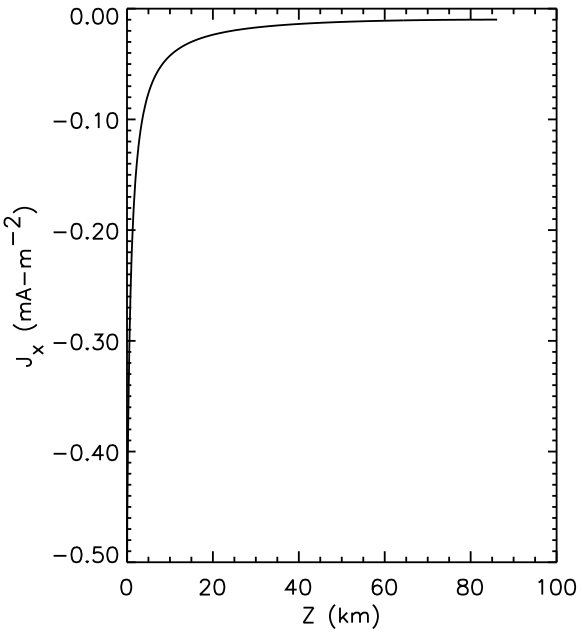


FIG. 10.—x component of current density vs. z. This is the largest component of the current density. $J_x \sim 10$–$10^2 J_y$. $J_z \equiv 0$.

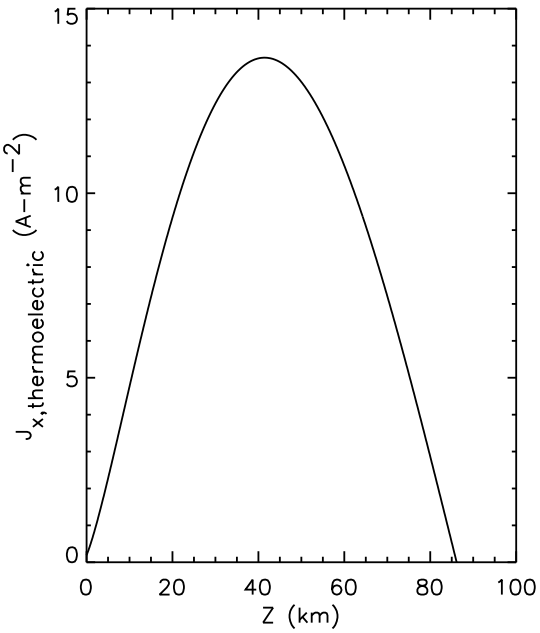


FIG. 12.—Thermoelectric part of J_x vs. z. This part of J_x is driven by the temperature gradient.

their sum J_y up to $z = 86$ km. At $z = 86.15$ km, where $J_{y,\text{thermoelectric}} = 0$, $J_{y,\text{conduction}} \sim 10^{-5}$ mA m^{-2}. Throughout the TR the thermoelectric current density is a major component of the current density. From equations (4) and (5) it follows that the high degree of cancellation of the x and y components of $\boldsymbol{J}_{\text{conduction}}$ and $\boldsymbol{J}_{\text{thermoelectric}}$ is connected to the near constancy of the magnetic field over the height range of the TR.

The results in this section strongly suggest that a large error in the computation of the current density and magnetic field occurs if the thermoelectric current density, or electron pressure gradient, are omitted from Ohm's law when modeling the TR.

4.2.4. *Current Dissipation*

The rate of current dissipation is $\boldsymbol{J}\cdot(\boldsymbol{E} + \boldsymbol{V} \times \boldsymbol{B}/c)$ and is shown in Figure 13. The NRL defined in equation (20) is shown in Figure 14. Comparison of Figures 13 and 14 shows that the observed radiation rate from the TR is $\sim 10^6$–10^{11} times larger than the rate of current dissipation. This result indicates that the contribution of in situ large-scale electric current dissipation to TR heating is insignificant.

The same result is expected from higher dimensional, time-dependent models for the following reason. The rate of current dissipation is determined by the temperature, density, electric and magnetic fields, and velocity. The

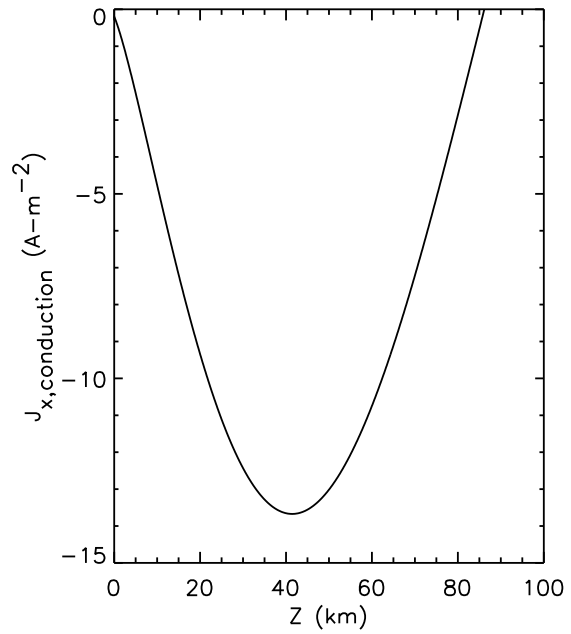


FIG. 11.—Conduction part of J_x vs. z. This part of J_x is driven by the effective electric field defined in eq. (13).

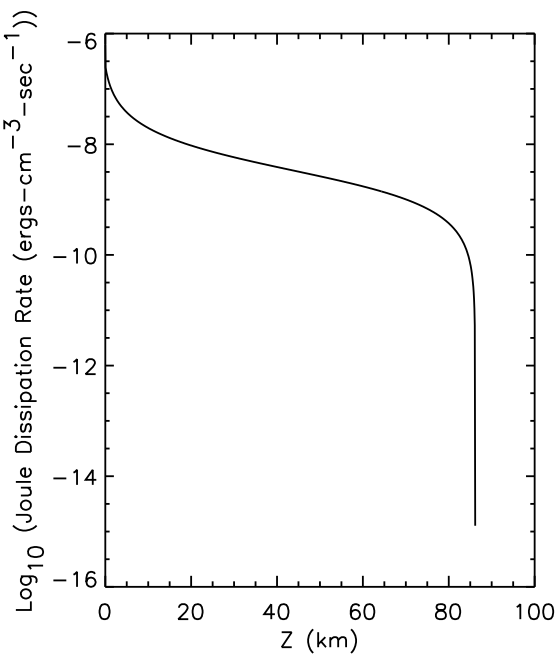


FIG. 13.—Logarithm of the Joule dissipation rate vs. z

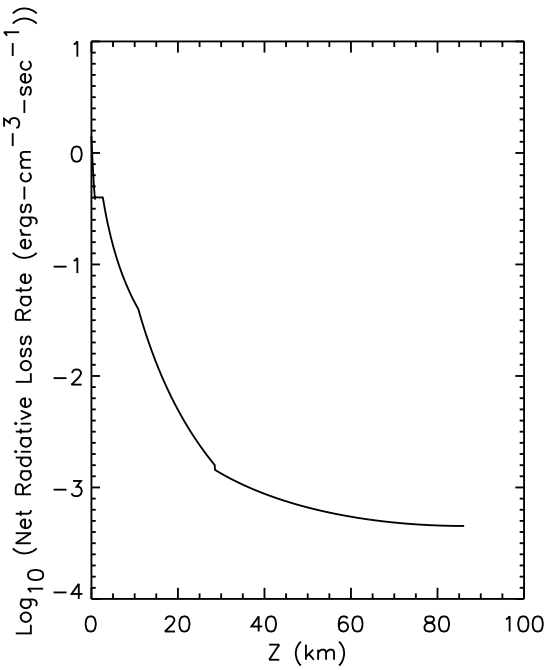


FIG. 14.—Logarithm of the net radiative loss rate vs. z. This profile is from Rosner et al. (1978).

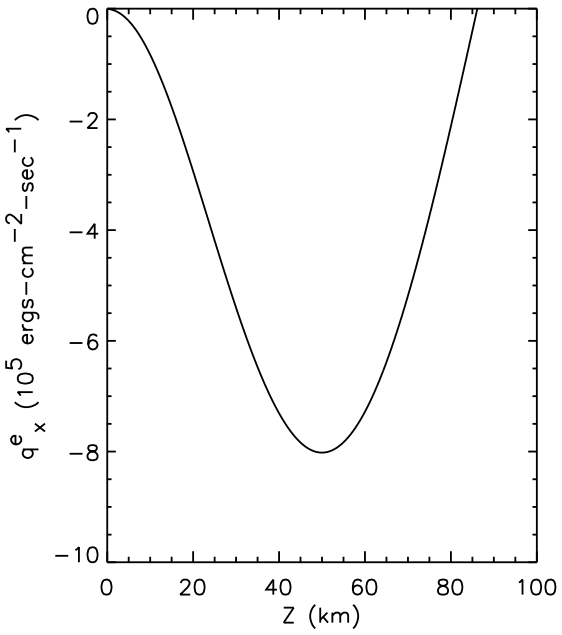


FIG. 15.—x component of electron heat flux vs. z. This is the largest component of the heat flux by a factor $\gtrsim 10$. The protons do not carry a significant heat flux.

values of these quantities input into and predicted by the present model are, with the possible exception of the electric field about which little is known, within the corresponding ranges currently believed to characterize the TR. Then, on the large scale, the magnitudes of these quantities generated by more realistic models cannot differ by many orders of magnitude from those in the present model. Therefore it is highly unlikely that the current dissipation rate predicted by more realistic models can be 6 or more orders of magnitude larger than that of the present model.

Although TR heating by large-scale electric current dissipation is negligible, substantial heating by small-scale electric current dissipation, believed to occur in current layers with a thickness ranging from several meters to about 1 km, might occur. Solutions exhibiting small-scale currents have so far not been found in the present model. It may be that they can be generated only by a higher dimensional model. A time-dependent model is probably not necessary in order to generate current sheets since they appear to be the end point of the asymptotic relaxation of the plasma toward a state of magnetostatic equilibrium (Parker 1994). A time-dependent model is necessary to describe the dynamics of the relaxation process but not the final dynamic steady state toward which the plasma evolves.

4.2.5. *Heat Flux*

The contribution of heat flux from the overlying corona to TR heating can be estimated by calculating the electron and proton heat fluxes defined in equations (17), (18), and (19). The x and z components of $\boldsymbol{q}^e$ are about 10 times larger than the corresponding components of $\boldsymbol{q}^p$. From $z = 0$ to $z \sim 12$ km, $q_y^e \sim q_y^p$. For $z > 12$ km, $q_y^e \sim 10 q_y^p$. It is found that $\boldsymbol{q}^e_{\text{thermoelectric}} \sim -0.5\boldsymbol{q}^e_{\text{conductive}}$ over almost the entire TR, so that the effective electric field drives a significant heat flux in a direction opposite to that driven by the temperature gradient. The vertical component of the thermoelectric heat flux flows toward the region of higher temperature and cancels $\sim 50\%$ of the vertical component of the temperature gradient–driven conductive heat flux that flows toward the region of lower temperature.

$\boldsymbol{q}^e$ is essentially parallel to $\boldsymbol{B}(\sim B_x\hat{\boldsymbol{x}})$. It is found that $q_x^e \sim 10^2 q_y^e$, and $\sim 10 q_z^e$. q_x^e and its conductive and thermoelectric components are shown in Figures 15, 16, and 17. It is the small vertical inclination of $\boldsymbol{B}$ by 1°.9 that allows the vertical temperature gradient to drive a conductive heat flux parallel to $\boldsymbol{B}$ with an average magnitude of $\sim 4.6 \times 10^5$ ergs cm^{-2} s^{-1}, which is close to the value of the NRL from the

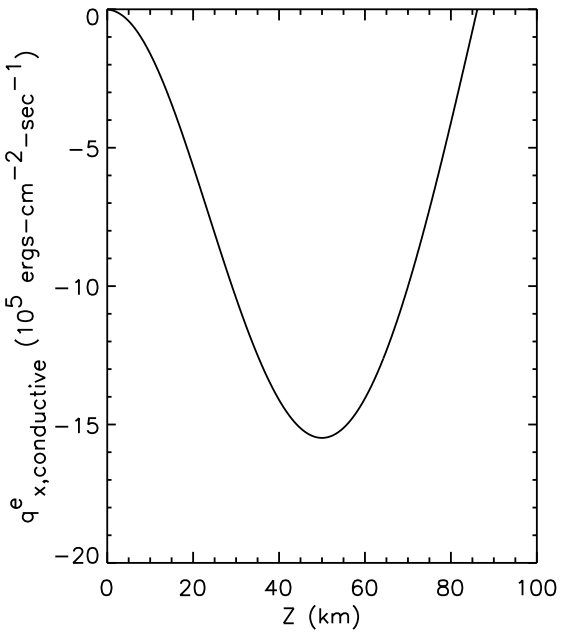


FIG. 16.—Conductive part of q_x^e vs. z. This part of q_x^e is driven by the temperature gradient.

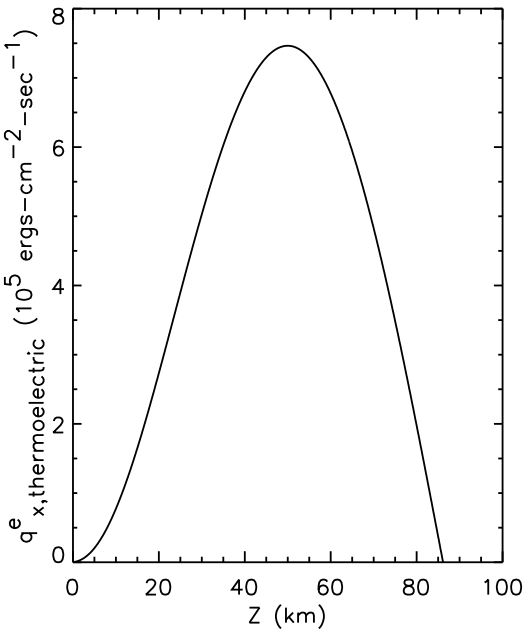


FIG. 17.—Thermoelectric part of q_x^e vs. z. This part of q_x^e is driven by the effective electric field.

TR of $\sim 4 \times 10^5$ ergs cm^{-2} s^{-1} inferred from observations. For comparison, the average values of q_y^e and q_z^e are $\sim -1.5 \times 10^3$ and -1.5×10^4 ergs cm^{-2} s^{-1}.

The orientation of the magnetic field with respect to the temperature gradient strongly affects the conductive and thermoelectric components of the electron heat flux. The reason for this is most easily seen by examining the expressions for the components of $\boldsymbol{q}^e$ when $\boldsymbol{B}$ is vertical ($\boldsymbol{B} = B_z \hat{\boldsymbol{z}}$), and when $\boldsymbol{B}$ is horizontal ($\boldsymbol{B} = B_x \hat{\boldsymbol{x}}$). When $\boldsymbol{B}$ is vertical,

$$q_x^e = T\left[\alpha_\perp\left(E_x + \frac{V_y B_z}{c}\right) + \alpha_\wedge\left(\alpha_z E_y - \frac{V_x B}{c}\right)\right] \quad (25)$$

$$q_y^e = T\left[\alpha_\perp\left(E_y - \frac{V_x B_z}{c}\right) - \alpha_\wedge\left(\alpha_z E_x + \frac{V_y B}{c}\right)\right] \quad (26)$$

$$q_z^e = T\alpha_\parallel\left(E_z + \frac{p'}{2en}\right) - \kappa_\parallel^e T' , \quad (27)$$

where $\alpha_z \equiv B_z/B = \pm 1$, and B is the magnitude of $\boldsymbol{B}$. When $\boldsymbol{B}$ is horizontal,

$$q_x^e = T\alpha_\parallel E_x \quad (28)$$

$$q_y^e = T\left\{\alpha_\wedge\left[\alpha_x\left(E_z + \frac{p'}{2en}\right) - \frac{V_y B}{c}\right] + \alpha_\perp\left(E_y + \frac{V_z B_x}{c}\right)\right\} - \alpha_x \kappa_\wedge^e T' \quad (29)$$

$$q_z^e = T\left[\alpha_\perp\left(E_z + \frac{p'}{2en} - \frac{V_y B_x}{c}\right) - \alpha_\wedge\left(\alpha_x E_y + \frac{V_z B}{c}\right)\right] - \kappa_\perp^e T' , \quad (30)$$

where $\alpha_x \equiv B_x/B = \pm 1$. If $(\omega_e \tau_e)^2 \gg 1$ (see Appendix A), then $\kappa_\parallel^e \gg |\kappa_\wedge^e| \gg \kappa_\perp^e$ and $|\alpha_\parallel| \gg \alpha_\perp \gg \alpha_\wedge$. For example, for solutions 1–3, $(\omega_e \tau_e)^2$ ranges from 10^5 at $z = 0$ to 10^{13} at $z = 86.15$ km, and the ranges of the components of the electron thermal conductivity and thermoelectric tensors from $z = 0$ to $z = 86.15$ km are, in the appropriate cgs units, $7.26 \times 10^4 \leq \kappa_\parallel^e \leq 7.67 \times 10^8$, $1.04 \geq \kappa_\perp^e \geq 9.72 \times 10^{-5}$, $-198.17 \leq \kappa_\wedge^e \leq -196.46$, $-7.57 \times 10^6 \geq \alpha_\parallel \geq -1.60 \times 10^9$, $58.42 \geq \alpha_\perp \geq 1.09 \times 10^{-4}$, and $0.47 \geq \alpha_\wedge \geq 8.27 \times 10^{-11}$. Similarly, the components of the electron conductivity tensor vary by several orders of magnitude over the height range of the TR. The large variation of the transport coefficients shows that it is not a good approximation to assume that they are constant.

When $\boldsymbol{B}$ is vertical, $\kappa_\parallel^e$ and $\alpha_\parallel$ occur only in q_z^e. In this case, a conductive heat flux with a magnitude comparable to the NRL of the TR can be driven along $\boldsymbol{B}$ by the temperature gradient, and a thermoelectric heat flux of comparable magnitude can be driven along $\boldsymbol{B}$ by the effective electric field. Since q_x^e and q_y^e involve only the much smaller transport coefficients $\kappa_\wedge^e$, $\kappa_\perp^e$, $\alpha_\wedge$, and $\alpha_\perp$, they are expected to be orders of magnitude smaller than q_z^e, provided a high degree of cancellation does not occur between $q_{z,\text{conductive}}^e$ and $q_{z,\text{thermoelectric}}^e$. This is essentially the case for solutions 1–3, which show that only a small vertical component of $\boldsymbol{B}$ is necessary in order for the basic features of this case to apply.

When $\boldsymbol{B}$ is horizontal, $\kappa_\parallel^e$ does not occur in any of the components of $\boldsymbol{q}^e$, and $\alpha_\parallel$ occurs only in q_x^e. The vertical heat flux tends to be strongly suppressed since it is much more difficult to drive a heat flux orthogonal to $\boldsymbol{B}$ than parallel to $\boldsymbol{B}$. In this case, it is unlikely that a conductive heat flux with a magnitude comparable to the NRL of the TR can flow in the plasma, but equation (28) suggests that a thermoelectric heat flux of this magnitude may be driven along $\boldsymbol{B}$ by the electric field. It is interesting to note that for the value of $\alpha_\parallel$ corresponding to a temperature of 10^6 K in solutions 1–3, equation (28) suggests that a parallel electric field strength of only $\sim 10^{-6}$ V m^{-1} is needed in order to drive a parallel heat flux of $\sim 10^5$ ergs cm^{-2} s^{-1}. Whether or not there are solutions to this, or a more realistic model in which such a small value of the electric field can drive such a large heat flux, remains to be determined.

Changes in the orientation of the magnetic field with respect to the temperature gradient may have a strong affect on TR heating because of the conductive heat flux from the corona. Changes in this orientation may be one of the causes of the observed fluctuations in the NRL from the TR. In the case of a vertical temperature gradient, a horizontal magnetic field strongly suppresses the thermal conduction of energy from the corona into the TR. If the magnetic field in the TR is primarily horizontal but has a small static or fluctuating vertical component, then a steady or fluctuating conductive heat flux large enough to balance the NRL from the TR may be driven from the corona along the magnetic field into the TR. Since the nearly horizontal magnetic field in solutions 1–3 represents the upper part of a magnetic loop in a closed field region of the TR, the conductive heat flux driven along this portion of the loop eventually flows down the nearly vertical sides of the loop through the TR. In this picture, the model predictions of the heat flux are consistent with the conclusion of Fontenla et al. (1993) and Macneice et al. (1991) that the electron heat flux from the corona, as determined by classical transport processes, is sufficient to heat the TR. However, it is necessary to include an energy equation in the model to determine the heat flux and temperature self-consistently in order to more accurately estimate the contribution of heat flux from the corona to TR heating.

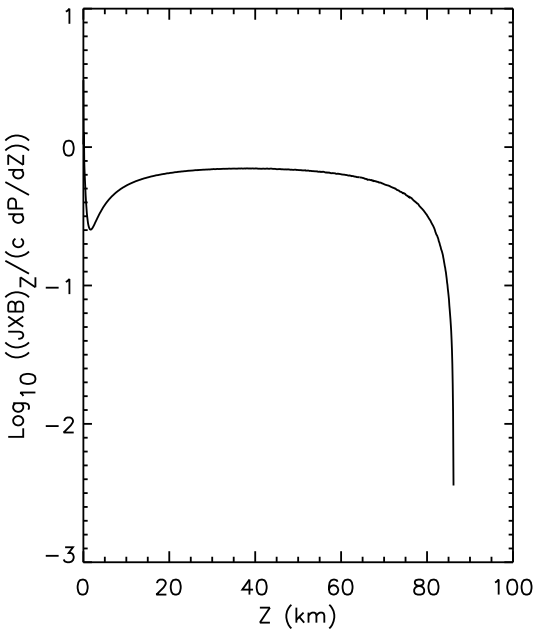


FIG. 18.—Logarithm of the ratio of the magnitude of the z component of the Lorentz force per unit volume to the magnitude of the pressure gradient vs. z.

4.2.6. *Force Free Assumption*

It is often assumed that the plasma in the TR is force free, defined by the condition that the ratio of the magnitude of each component of the Lorentz force per unit volume $\boldsymbol{J} \times \boldsymbol{B}/c$ to the magnitude of the corresponding component of ∇p is $\ll 1$. For the model considered here, the relevant ratio is $|(\boldsymbol{J} \times \boldsymbol{B})_z/(cp')|$. This ratio is shown in Figure 18. The ratio is ~ 1 at the base of the TR, dips to ~ 0.25, and then increases, remaining $\gtrsim 0.5$ for $10 \lesssim z \lesssim 73$ km, and then rapidly decreases to values $\ll 1$. The average value of the ratio is ~ 0.56. These results suggest that the force free approximation is not valid over most of the TR and hence that the Lorentz force plays an important role in momentum conservation in the TR.

5. CONCLUSIONS

The dissipation of large-scale electric currents is not a significant source of heating for the TR. The negligible value of the current dissipation rate $\boldsymbol{J} \cdot (\boldsymbol{E} + \boldsymbol{V} \times \boldsymbol{B}/c)$ appears to be due to two factors. The first is the smallness of the magnitude of $\boldsymbol{E} + \boldsymbol{V} \times \boldsymbol{B}/c$ ($\sim 10^{-6}$ V m^{-1}). The second is the cancellation of the conduction and thermoelectric components of the current density to 1 part in 10^4–10^5 over almost the entire TR. The small value of the current dissipation rate may be an example of the principle of minimum energy dissipation, which states that a plasma evolves to a state in which the rate at which dissipative processes generate thermal energy is the minimum value consistent with the constraints on the plasma. For the model considered here, the state is an equilibrium state, and the constraints are the input values of the boundary conditions and parameters.

Provided the magnetic field in the TR has a steady or fluctuating vertical component, the conductive electron heat flux from the corona into the TR flows parallel to the magnetic field and may provide the energy necessary to balance the NRL from the TR. A significant fraction of the conductive heat flux is cancelled by a thermoelectric heat flux driven by the effective electric field. The electron pressure gradient makes a major contribution to this electric field. The thermoelectric heat flux flows toward the region of higher temperature but does not exceed the conductive heat flux, which flows toward the region of lower temperature.

It is necessary to include thermoelectric and electron pressure gradient effects in Ohm's law and in the expression for the electron heat flux in order to accurately model the current density, magnetic field, and electron heat flux in the TR. This is expected to be true on all spatial scales, in particular on the small scales conjectured to characterize current sheets and thin filaments. The force free approximation is probably not valid in the TR in the sense that although the current density is nearly parallel to the magnetic field, the Lorentz force is not necessarily small compared with the pressure gradient in the momentum equation.

The results on heating of the TR are consistent with the current view that the TR is heated in situ on small spatial scales, or by thermal energy flux from the corona, or by some combination of the two. The results indicate that, if in situ heating is important in the TR, then it is due to viscous dissipation or the dissipation of small scale electric currents. Future modeling of current dissipation in current sheets or thin filaments using classical transport coefficients may provide an accurate, quantitative measure of the importance of small-scale current dissipation in in situ heating of the TR. On the meter to kilometer scales believed to characterize small scale electric currents, anomalous transport processes might dominate over classical transport processes. An important step toward determining whether or not this is the case is to model these currents using classical transport coefficients and then check if the condition $E_{\|}/E_D \ll 0.21$ is violated.

Viscous dissipation is not included in the model. Its contribution to TR heating on large and small scales remains to be determined. It is likely that this contribution is largest on small scales where the largest velocity gradients probably occur.

The electric field plays an important role in determining the current density and the heat flux through thermoelectric effects. In order to understand how the TR and corona are heated, it is necessary to know the electric field. Therefore it is critically important to model the effects of the electric field on the dissipation and transport of energy in the solar atmosphere in a realistic manner. This can be done only by using models that include a realistic representation of transport processes and that compute the electric field self-consistently. In particular, these models should allow for the computation of $\boldsymbol{E} + \boldsymbol{V} \times \boldsymbol{B}/c$, and of the corresponding Stark splitting in neutral hydrogen in thin current layers. This splitting may be detected in observations of line broadening in neutral hydrogen.

The model presented here is based on the validity of the classical transport coefficients in the TR. The discussion in § 2.1 indicates that classical transport processes are dominant in the LTR and probably play an important though perhaps not dominant role in the UTR. Since most of the NRL from the TR comes from the LTR, and since the classical transport coefficients are the only transport coefficients known explicitly in terms of MHD variables, they provide the only available, largely realistic description of

transport processes in the TR. The classical transport coefficients for a partially ionized hydrogen plasma (Mitchner & Kruger 1973) may be used in MHD models to obtain important information about energy dissipation and transport in the solar chromosphere (Goodman 1997b). It is also important to note that the solar interior is a fully ionized, strongly collision-dominated plasma, so that the use of classical transport coefficients in MHD models of the solar interior is expected to provide important insight into the dynamo mechanism.

The importance of using realistic descriptions of transport processes in modeling the solar atmosphere cannot be overemphasized. Although the development of such models is necessary for identifying and understanding heating and wind acceleration mechanisms in the solar atmosphere, very little work has been done in this area. Existing multidimensional, time-dependent MHD models of the solar atmosphere cannot use even remotely realistic descriptions of transport processes because their use requires computational speeds that exceed what is available by many orders of magnitude. Although essential for modeling the multidimensional, large-scale dynamics of the solar atmosphere, these models must be complemented by lower dimensional, time-independent and -dependent models in which it is practical to use realistic descriptions of transport processes, whether classical or anomalous.

The author thanks Stuart D. Jordan in the Laboratory for Astronomy and Solar Physics at NASA/Goddard and Vladimir Airapetian in the System Sciences Division of Computer Sciences Corporation for important discussions of the material presented in this manuscript. The author thanks the anonymous referee for constructive criticism that led to significant improvement of the manuscript. The author also thanks Steven A. Curtis and William H. Mish in the Laboratory for Extraterrestrial Physics at NASA/Goddard for support of this work.

APPENDIX A

TRANSPORT COEFFICIENTS

The expressions for the transport coefficients are taken directly from Balescu (1988a). They are valid for all values of $\omega_e\tau_e$, where ω_e and τ_e are the electron cyclotron frequency and electron-proton collision time. For the expressions given below the ion charge and mass are set equal to the proton charge and mass, and the electron and ion temperatures are assumed to be equal.

A1. ELECTRICAL CONDUCTIVITY TENSOR

The components of the electrical conductivity tensor $\boldsymbol{\sigma}$ are

$$\sigma_{\parallel,\perp,\wedge} = \frac{e^2 n\tau_e}{m_e}\,\tilde{\sigma}_{\parallel,\perp,\wedge}\,, \tag{A1}$$

where

$$\tilde{\sigma}_{\parallel} = 1.932 \tag{A2}$$

$$\tilde{\sigma}_{\perp} = \frac{(1.8 + (\omega_e\tau_e)^2)}{[0.933 + 6.28(\omega_e\tau_e)^2 + (\omega_e\tau_e)^4]} \tag{A3}$$

$$\tilde{\sigma}_{\wedge} = \frac{(\omega_e\tau_e)(4.38 + (\omega_e\tau_e)^2)}{[0.933 + 6.28(\omega_e\tau_e)^2 + (\omega_e\tau_e)^4]} \tag{A4}$$

and

$$\tau_e = \frac{3m_e^{1/2}(k_{\rm B}T)^{3/2}}{4(2\pi)^{1/2}e^4 n\ln\lambda} \tag{A5}$$

$$\lambda = \frac{3(k_{\rm B}T)^{3/2}}{2e^3(\pi n)^{1/2}}\,. \tag{A6}$$

$\sigma_{\wedge}$ is the Hall conductivity, λ is the Coulomb logarithm, and m_e is the electron mass.

A2. THERMOELECTRIC TENSOR

The components of the thermoelectric tensor $\boldsymbol{\alpha}$ are

$$\alpha_{\parallel,\perp,\wedge} = \frac{en\tau_e 2.5^{1/2}}{m_e}\,\tilde{\alpha}_{\parallel,\perp,\wedge}\,, \tag{A7}$$

where

$$\tilde{\alpha}_{\parallel} = -0.982 k_{\mathrm{B}} \tag{A8}$$

$$\tilde{\alpha}_{\perp} = \frac{-0.949 k_{\mathrm{B}}(0.966 - (\omega_e \tau_e)^2)}{[0.933 + 6.28(\omega_e \tau_e)^2 + (\omega_e \tau_e)^4]} \tag{A9}$$

$$\tilde{\alpha}_{\wedge} = \frac{-2.719 k_{\mathrm{B}}(\omega_e \tau_e)}{[0.933 + 6.28(\omega_e \tau_e)^2 + (\omega_e \tau_e)^4]} . \tag{A10}$$

A3. ELECTRON THERMAL CONDUCTIVITY TENSOR

The components of the electron thermal conductivity tensor $\boldsymbol{\kappa}^e$ are

$$\kappa^e_{\parallel,\perp,\wedge} = \frac{2.5 n k_{\mathrm{B}} T \tau_e}{m_e} \tilde{\kappa}^e_{\parallel,\perp,\wedge} , \tag{A11}$$

where

$$\tilde{\kappa}^e_{\parallel} = 1.036 k_{\mathrm{B}} \tag{A12}$$

$$\tilde{\kappa}^e_{\perp} = \frac{k_{\mathrm{B}}(0.966 + 1.866(\omega_e \tau_e)^2)}{[0.933 + 6.28(\omega_e \tau_e)^2 + (\omega_e \tau_e)^4]} \tag{A13}$$

$$\tilde{\kappa}^e_{\wedge} = \frac{k_{\mathrm{B}}(\omega_e \tau_e)(1.9 + (\omega_e \tau_e)^2)}{[0.933 + 6.28(\omega_e \tau_e)^2 + (\omega_e \tau_e)^4]} . \tag{A14}$$

A4. PROTON THERMAL CONDUCTIVITY TENSOR

The components of the proton thermal conductivity tensor $\boldsymbol{\kappa}^p$ are

$$\kappa^p_{\parallel,\perp,\wedge} = \frac{2.5 n k_{\mathrm{B}} T \tau_p}{m_p} \tilde{\kappa}^p_{\parallel,\perp,\wedge} , \tag{A15}$$

where

$$\tilde{\kappa}^p_{\parallel} = 1.768 k_{\mathrm{B}} \tag{A16}$$

$$\tilde{\kappa}^p_{\perp} = \frac{0.566 k_{\mathrm{B}}}{0.32 + (\omega_p \tau_p)^2} \tag{A17}$$

$$\tilde{\kappa}^p_{\wedge} = \frac{(\omega_p \tau_p) k_{\mathrm{B}}}{0.32 + (\omega_p \tau_p)^2} \tag{A18}$$

and

$$\tau_p = \left(\frac{m_p}{m_e}\right)^{1/2} \tau_e . \tag{A19}$$

Here ω_p and τ_p are the proton cyclotron frequency and the proton-proton collision time.

APPENDIX B

EXPRESSIONS FOR $F_i (1 \le i \le 3)$

Define

$$\Gamma = \frac{1}{[(\sigma_{\parallel} - \sigma_{\perp})\alpha_z^2 + \sigma_{\perp}]} \left([(\alpha_{\parallel} - \alpha_{\perp})\alpha_z^2 + \alpha_{\perp}] T' - (\sigma_{\parallel} - \sigma_{\perp})\alpha_z(\alpha_x E_x + \alpha_y E_y) \right.$$
$$\left. - \frac{\sigma_{\perp}}{c}(V_x B_y - V_y B_x) - \sigma_{\wedge} \left\{ E_x \alpha_y - E_y \alpha_x - \frac{B}{c} \left[(1 - \alpha_z^2) \frac{2 k_{\mathrm{B}} T M_0}{m_p p} - \alpha_z (V_x \alpha_x + V_y \alpha_y) \right] \right\} \right) , \tag{B1}$$

where

$$\alpha_x = \frac{B_x}{B} \tag{B2}$$

$$\alpha_y = \frac{B_y}{B} \tag{B3}$$

$$\alpha_z = \frac{B_z}{B} \tag{B4}$$

and B is the magnitude of $\boldsymbol{B}$. Then the expressions for the derivatives of B_x, B_y, and p in equations (22), (23), and (24) are, respectively, given by:

$$F_1 = \frac{4\pi}{c}\left([(\sigma_{\|}-\sigma_{\perp})\alpha_y\alpha_z + \sigma_{\wedge}\alpha_x]\Gamma - [(\alpha_{\|}-\alpha_{\perp})\alpha_z\alpha_y + \alpha_{\wedge}\alpha_x]T' + (\sigma_{\|}-\sigma_{\perp})\alpha_y(\alpha_x E_x + \alpha_y E_y)\right.$$
$$\left. + \sigma_{\perp}\left[E_y + \frac{1}{c}\left(\frac{2k_{\rm B}TM_0B_x}{m_p p} - V_x B_z\right)\right] - \sigma_{\wedge}\left\{E_x\alpha_z + \frac{B}{c}\left[V_y(1-\alpha_y^2) - \alpha_y\left(V_x\alpha_x + \frac{2k_{\rm B}TM_0\alpha_z}{m_p p}\right)\right]\right\}\right), \tag{B5}$$

$$F_2 = \frac{-4\pi}{c}\left([(\sigma_{\|}-\sigma_{\perp})\alpha_x\alpha_z - \sigma_{\wedge}\alpha_y]\Gamma - [(\alpha_{\|}-\alpha_{\perp})\alpha_z\alpha_x - \alpha_{\wedge}\alpha_y]T' + (\sigma_{\|}-\sigma_{\perp})\alpha_x(\alpha_x E_x + \alpha_y E_y)\right.$$
$$\left. + \sigma_{\perp}\left[E_x - \frac{1}{c}\left(\frac{2k_{\rm B}TM_0B_y}{m_p p} - V_y B_z\right)\right] + \sigma_{\wedge}\left\{E_y\alpha_z - \frac{B}{c}\left[V_x(1-\alpha_x^2) - \alpha_x\left(V_y\alpha_y + \frac{2k_{\rm B}TM_0\alpha_z}{m_p p}\right)\right]\right\}\right), \tag{B6}$$

and

$$F_3 = \frac{m_p p^2}{(2k_{\rm B}TM_0^2 - m_p p^2)}\left[(2k_{\rm B}T' + g_{\odot}m_p)\frac{p}{2k_{\rm B}T} + \frac{1}{4\pi}(B_x F_1 + B_y F_2)\right] + \frac{pT'}{T}, \tag{B7}$$

where V_x and V_y are given by equations (8) and (9) in terms of $V_x(0)$, $V_y(0)$, $B_x(0)$, $B_y(0)$, M_0, and B_z.

REFERENCES

Anderson, S. W. 1994, ApJ, 437, 860
Anderson, S. W., Raymond, J. C., & Van Ballegooijen, A. 1996, ApJ, 457, 939
Athay, R. G., & Dere K. P. 1991, ApJ, 381, 323
Balescu, R. 1988a, Transport Processes in Plasmas, Vol. 1 (New York: North Holland)
———. 1988b, Transport Processes in Plasmas, Vol. 2 (New York: North Holland)
Book, D. L. 1990, NRL Plasma Formulary (Washington, DC: Naval Res. Lab.)
Braginskii, S. I. 1965, Transport Processes in a Plasma. Reviews of Plasma Physics, ed. M. A. Leontovich, Vol. 1 (New York: Consultants Bureau), 205
Brosius, J. W., Davila, J. M., Thomas, R. J., & Monsignori-Fossi, B. C. 1996, ApJS, 106, 143
Brynildsen, N., Kjeldseth-Moe, O., & Maltby, P. 1996, ApJ, 462, 534
de Kluiver, H., Perepelkin, N. F., & Hirose, A. 1991, Phys. Rep., 199, 281
Dere, K. P., Bartoe, J.-D. F., & Brueckner, G. E. 1984, ApJ, 281, 870
Dowdy, J. F., Jr. 1993, ApJ, 411, 406
Dowdy, J. F., Jr., Rabin, D., & Moore, R. L. 1986, Sol. Phys., 105, 35
Dreicer, H. 1959, Phys. Rev., 115, 238
Fontenla, J. M., Avrett, E. H., & Loeser, R. 1991, ApJ, 377, 712
———. 1993, ApJ, 406, 319
Foukal, P. 1990, Solar Astrophysics (New York: Wiley)
Foukal, P., & Hinata, S. 1991, Sol. Phys., 132, 307
Goodman, M. L. 1995, ApJ, 443, 450
———. 1996, ApJ, 463, 784
———. 1997a, A&A, 324, 311
———. 1997b, A&A, 325, 341
Landini, E., & Landini, M. 1997, A&A, 327, 1230
Macneice, P., Fontenla, J., & Ljepojevic, N. N. 1991, ApJ, 369, 554
Mariska, J. T. 1986, ARA&A, 24, 23
———. 1988, ApJ, 334, 489
———. 1992, The Solar Transition Region, Cambridge Astrophysics Series (Cambridge: Cambridge Univ. Press)
Mitchner, M., & Kruger, C.H. 1973, Partially Ionized Gases, Wiley Series in Plasma Physics (New York: Wiley)
Parker, E. N. 1994, Spontaneous Current Sheets in Magnetic Fields, International Series on Astronomy and Astrophysics (Oxford: Oxford Univ. Press)
Press, W. H., Teukolsky, S. A., Vetterling, W. T., & Flannery, B. P. 1992, Numerical Recipes in Fortran (New York: Cambridge Univ. Press)
Rabin, D., & Dowdy, J. F., Jr. 1992, ApJ, 398, 665
Rabin, D., & Moore, R. L. 1984, ApJ, 285, 359
Rosner, R., Tucker, W. H., & Vaiana, G. S. 1978, ApJ, 220, 643
Scudder, J. D. 1994, ApJ, 427, 446
Vaiana, G. S., Krieger, A. S., & Timothy, A. F. 1973, Sol. Phys., 32, 81
Warren, H. P., Mariska, J. T., Wilhelm, K., & Lemaire, P. 1997, ApJ, 484, L91